Author/s:
Du, Y;Brown, JR;Menviel, L;Saini, H;Drysdale, RN

Title:
The Impacts of an AMOC Slowdown on Southern Hemisphere and Australian Climates at 8.2 ka in ACCESS-ESM1.5 Model

Date:
2025-04-28

Citation:
Du, Y., Brown, J. R., Menviel, L., Saini, H. & Drysdale, R. N. (2025). The Impacts of an AMOC Slowdown on Southern Hemisphere and Australian Climates at 8.2 ka in ACCESS-ESM1.5 Model. Journal of Geophysical Research (JGR): Atmospheres, 130 (8), https://doi.org/10.1029/2024JD042432.

Persistent Link:
https://hdl.handle.net/11343/362585

JGR Atmospheres

RESEARCH ARTICLE
10.1029/2024JD042432

The Impacts of an AMOC Slowdown on Southern Hemisphere and Australian Climates at 8.2 ka in ACCESS-ESM1.5 Model

Yanxuan Du[1], Josephine R. Brown[1], Laurie Menviel[2,3], Himadri Saini[2,3], and Russell N. Drysdale[1]

[1]School of Geography, Earth and Atmospheric Sciences, University of Melbourne, Parkville, VIC, Australia, [2]Climate Change Research Centre, University of New South Wales, Sydney, NSW, Australia, [3]The Australian Centre for Excellence in Antarctic Science, University of New South Wales, Sydney, NSW, Australia

Key Points:

- Our model suggests that the 8.2 ka event is likely to be caused by a combined effect of lake drainage and ice melting over the Hudson Bay
- Southern Hemisphere climate displays significant changes to a weakened Atlantic Meridional Overturning Circulation (AMOC) at 8.2 ka
- Northern Australia is cooler and wetter while southern Australia is warmer and drier due to AMOC weakening

Supporting Information:

Supporting Information may be found in the online version of this article.

Correspondence to:

Y. Du,
yanxuand@student.unimelb.edu.au

Citation:

Du, Y., Brown, J. R., Menviel, L., Saini, H., & Drysdale, R. N. (2025). The impacts of an AMOC slowdown on southern hemisphere and australian climates at 8.2 ka in ACCESS-ESM1.5 model. *Journal of Geophysical Research: Atmospheres*, *130*, e2024JD042432. https://doi.org/10.1029/2024JD042432

Received 13 SEP 2024
Accepted 22 MAR 2025

Author Contributions:

Conceptualization: Yanxuan Du, Josephine R. Brown, Laurie Menviel
Data curation: Yanxuan Du
Formal analysis: Yanxuan Du
Funding acquisition: Josephine R. Brown, Laurie Menviel, Russell N. Drysdale
Investigation: Yanxuan Du
Methodology: Yanxuan Du, Himadri Saini
Project administration: Josephine R. Brown, Russell N. Drysdale
Resources: Yanxuan Du, Josephine R. Brown
Software: Yanxuan Du, Himadri Saini

Abstract Greenland ice cores reveal an abrupt cooling of up to 3.3°C 8.2 kyr ago (8.2 ka), lasting for roughly 160 years. The event was likely caused by a weakening of the Atlantic Meridional Overturning Circulation (AMOC) due to freshwater drainage into the North Atlantic. It was associated with a global-scale climate change but is recorded in very few high-resolution paleoclimatic time series from the Southern Hemisphere (SH). In this study, we investigate the 8.2 ka event in the SH, particularly the Australian climate response to a weakened AMOC. Five North Atlantic meltwater experiments are conducted with the Australian Earth System Model, ACCESS-ESM1.5, to evaluate the sensitivity of AMOC responses to freshwater perturbations under early Holocene conditions as well as their climate impact. Our results suggest a 100 year freshwater pulse reproduces a global climate change that best matches existing proxy records for the 8.2 ka event. Australian surface air temperatures show significant cooler conditions in the northern half of the continent but warmer anomalies in the south in response to a weakened AMOC. Australian hydroclimate displays a more complex response at 8.2 ka. Northern Australian precipitation is influenced by a southward shift in the mean position of the Intertropical Convergence Zone and a strengthened Indo-Australian summer monsoon, while the southern part of the continent is more sensitive to weakening of the winter westerly winds. These results highlight the importance of understanding the Australian climate response to a weakened AMOC under different background climate in order to better predict potential future impacts.

Plain Language Summary The latest abrupt cooling event in Earth's history happened around 8,200 years ago (8.2 ka). This event is associated with a global climate change that lasted roughly 160 years; however, it is mostly evident in Northern Hemisphere records. The Southern Hemisphere (SH) response is inconsistent in both paleoclimate records and model simulations. This event is believed to be associated with a weakened northward ocean heat transport in the Atlantic Ocean (via the Atlantic Meridional Overturning Circulation (AMOC)). In this study, we use a version of the Australian Community Climate and Earth System Simulator model, ACCESS-ESM1.5, to investigate the climate response over the SH, particularly Australian region, to North Atlantic freshwater forcing (FWF) at 8.2 ka. We perform five different freshwater perturbation experiments to test model behaviors. Only the long-term FWF simulation reproduces similar responses as in paleoclimate records. In that experiment, northern Australia is simulated to have cooler conditions with enhanced annual precipitation, while the southern part of the continent is warmer and drier. Changes in seasonal atmospheric circulations greatly influence the precipitation patterns over Australia at 8.2 ka. These results provide important information regarding the potential impacts of future AMOC weakening on Australian climate.

1. Introduction

Approximately 8.2 kyr ago (8.2 ka), ice-core records show that Greenland experienced the largest abrupt cooling event of the past 12,000 years (Vinther et al., 2006). During this "8.2 ka event" (Alley et al., 1997), the temperature over Greenland decreased by 3.3°C ± 1.1°C (Kobashi et al., 2007), whilst large parts of the Northern Hemisphere (NH) high latitudes experienced a 1°C–3°C cooling for a duration of around 160 years (Boch et al., 2009; Nicolussi & Schluchter, 2012; Thomas et al., 2007). The original hypothesis for the cause of the 8.2 ka event is that deglacial meltwaters during the early Holocene formed the proglacial Lakes Agassiz and Ojibway until ultimately the ice dam over the Hudson Bay collapsed, leading to a catastrophic outburst into the Labrador

Supervision: Josephine R. Brown, Laurie Menviel, Russell N. Drysdale
Validation: Josephine R. Brown, Laurie Menviel
Visualization: Yanxuan Du
Writing – original draft: Yanxuan Du
Writing – review & editing: Josephine R. Brown, Laurie Menviel, Himadri Saini, Russell N. Drysdale

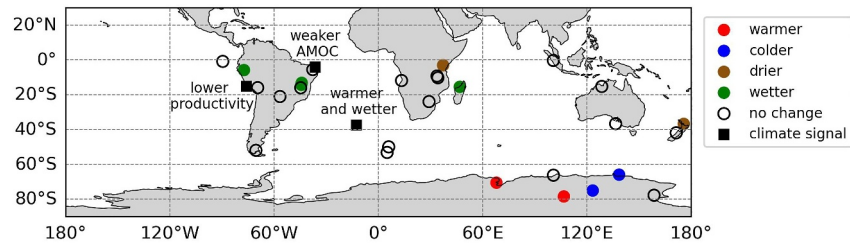

Figure 1. Summary of Southern Hemisphere (SH) climate signals for the 8.2 ka event (detailed site information is provided in Tables S1 and S2 in Supporting Information S1). These includes: inferred temperature and precipitation anomalies for the 8.2 ka event from Morrill, Anderson, et al. (2013) synthesis, speleothem records from Speleothem Isotope and Analysis (SISAL) v2 database analyzed by Parker and Harrison (2022), and two new SH records from the SISAL v3 database (Kaushal et al., 2024). Unfilled circles indicate sites with no anomalies detected.

Sea (Hoffman et al., 2012; Teller et al., 2002). This freshened the North Atlantic, slowed down deep-water formation, thus weakening the Atlantic Meridional Overturning Circulation (AMOC), which controls inter-hemispheric ocean heat transport (Buckley & Marshall, 2016). Consequently, there was a cooling over the North Atlantic region. However, some studies have proposed that the 8.2 ka event was not solely caused by a lake outburst but was also due to a combination of accelerated ice melting from the collapse of the NH Laurentide ice saddle over the Hudson Bay (e.g., Aguiar et al., 2021; Carlson et al., 2009; Gregoire et al., 2012).

Many modeling studies have conducted sensitivity tests of freshwater perturbations to understand the cause of the event and to reproduce the cooling estimated from paleo-data reconstructions (Clarke et al., 2009; LeGrande & Schmidt, 2008; Li et al., 2009; Matero et al., 2017; Morrill et al., 2014; Renssen et al., 2001, 2002; Tindall & Valdes, 2011; Wagner et al., 2013; Wiersma et al., 2006; Wiersma & Renssen, 2006). Previous experiments were designed to either simulate the "lake outburst", which is to add a large flux of typically 2.5 Sv for 1 year following the Paleoclimate Modelling Intercomparison Project (PMIP) protocols (Otto-Bliesner et al., 2017), or to reproduce a "lake + ice collapse" simulation, for which a peak flux is added for 1 year, accompanied by a continuous small flux for ∼100 years to mimic the ice melting. Previous modeling studies all suggest that the lake drainage alone does not reproduce the duration of anomalous cooling as preserved in the Greenland ice records. Most models show AMOC reduction lasting only decades with lake release simulations (e.g., Wagner et al., 2013; Wiersma et al., 2006; Wiersma & Renssen, 2006). Instead, a ∼100 year release of meltwater flux from the collapse of the Hudson Bay and lake outburst together is more likely to reproduce the amplitude and duration of the cooling anomalies that best match the proxy records (e.g., Matero et al., 2017; Wagner et al., 2013), although the AMOC response has been found to be highly model-dependent. Different model resolution, location of the freshwater input, and duration of the lake release could impact the simulation results (e.g., Shi et al., 2020; Wagner et al., 2013). Previous modeling studies have focused mainly on NH climate anomalies since most of the paleoclimate data is from the NH and they display a more consistent climate response. Few modeling studies have investigated whether there is a consistent signal of the 8.2 ka event in the Southern Hemisphere (SH) including over Australia.

There are a small number of high-resolution proxy records available globally for the 8.2 ka event, with fewer for the SH, which show less consistency and large regional diversity (Morrill, Anderson, et al., 2013). Proxy records show evidence of drier conditions over Greenland, Asia, southern Europe, Central America, northern South America, and parts of southern Africa during the 8.2 ka event, with some sites suggesting a strengthened Asian winter monsoon, and enhanced precipitation in the SH tropics (Morrill, Anderson, et al., 2013). Parker and Harrison (2022) analyzed high-resolution speleothem records covering the Holocene epoch from the Speleothem Isotope and Analysis (SISAL) version 2 database (Comas-Bru et al., 2020), which includes two sites in the Australian and Maritime continents (Denniston et al., 2013; Wurtzel et al., 2018); however, no distinct 8.2 ka signal was found after performing the breakpoint analysis (as indicated in Figure 1). Two new SH records (Azevedo et al., 2021; Utida et al., 2020) from SISAL v3 database (Kaushal et al., 2024) are also included; however, there is no evidence for the 8.2 ka event. A southward shift of the mean position of the Inter-Tropical Convergence Zone (ITCZ) was suggested from the negative oxygen isotope signals in the SH tropics and drier conditions in Asia, although there is a lack of signals in the Indo-Australian monsoon region (Figure 1). Lake sediments from Auckland, New Zealand, suggest drier conditions accompanied with increased storminess around

8,240 cal yr BP, which could be a response to the freshwater drainage event at 8.2 ka (Augustinus et al., 2008). However, no 8.2 ka signals were detected from speleothem record in the Metro Cave to the south of Auckland (Logan, 2011). Due to the lack of temperature anomalies in SH proxy records, with Antarctic ice core records (Figure 1), it is uncertain whether a bipolar seesaw response (Stocker & Johnsen, 2003) was established during the 8.2 ka event.

Proxy records also do not provide a clear picture of possible changes in the SH westerly winds (SWW). De Deckker (2022) synthesized well-dated Holocene proxies along eastern Australia, suggesting largely weakened westerlies offshore southern Australia between ∼8.2 and ∼5.5 ka. Zwier et al. (2024) reconstructed SH westerlies from lake sediments on the Kerguelen Islands and pollen and microcharcoal from southern Africa, which revealed a northward shift of the core belt of the SWW starting at 8,600 cal yr BP. Zwier et al. (2024) proposed that the changes might be due to the 8.2 ka cooling event, although identifiable changes in the SWW were found from neither sub-Antarctic South Georgia pollen records (Zwier et al., 2022) nor regional South Atlantic reconstructions (Tamhane et al., 2023).

There are many challenges in identifying the 8.2 ka event from proxy records, as the event is short enough that any climate anomalies near 8.2 ka could be an indication of the event or could be uncorrelated multi-decadal climate variability. Uncertainties and discrepancies still exist among high-resolution records. Some studies argue that the anomalies in the proxy records near 8.2 ka show two phases of the event with a ∼69 year central event during the full event of ∼160 years (Rohling & Pälike, 2005; Thomas et al., 2007). In addition, it is unclear in both the proxy data and previous model simulations whether the freshwater forcing (FWF) in the North Atlantic at 8.2 ka was large enough to cause changes in meridional oceanic heat transport significant enough to warm the SH, as happened during Dansgaard-Oeschger and Heinrich stadials (Menviel et al., 2020; Stocker & Johnsen, 2003).

Here, we provide a detailed analysis of simulated climate responses over the SH, with a particular focus on the Australian region, to an AMOC weakening consistent with the 8.2 ka event using the Australian Community Climate and Earth System Simulator (ACCESS) Earth System Model (ESM) version 1.5. A systematic assessment of the possible meltwater fluxes that would lead to an agreement with the NH proxy records for the 8.2 ka event is conducted. This also allows us to examine the sensitivity of the AMOC response to freshwater perturbations in this model. A discussion of how the modeling results compare to proxy data is also provided.

2. Methods

2.1. The Climate Model: ACCESS-ESM1.5

This study makes use of the Australian Community Climate and Earth System Simulator (ACCESS) ESM version 1.5, which is one of the two model versions (ACCESS-ESM1.5 and ACCESS-CM2) that participated in the Coupled Model Intercomparison Project Phase 6 (CMIP6) with an interactive carbon cycle (Ziehn et al., 2020). The resolution of the atmospheric model component (UK Met Office Unified Model, UM) is 1.875° × 1.25° (Martin et al., 2010; The HadGEM2 Development Team: G. M. Martin et al., 2011), coupled to the land surface model, which is the Community Atmosphere Biosphere Land Exchange model (Kowalczyk et al., 2013). The ocean and sea ice components are coupled with a common horizontal grid of 360 × 300 cells with 1° resolution (Griffies, 2012; Hunke & Lipscomb, 2010; respectively). More details of model description are provided in Ziehn et al. (2020). The AMOC sensitivity to freshwater perturbations is within the range of CMIP6 models tested in historical and future scenarios (Weijer et al., 2020).

The ACCESS-ESM1.5 model has performed a set of standard "DECK" experiments (Eyring et al., 2016) and historical simulations in order to participate in CMIP6 (Mackallah et al., 2022). The model is also included as one of the Paleoclimate Model Intercomparison Project phase 4 (PMIP4) models that performed standard paleoclimate simulations, including the Last Interglacial (lig127k; Yeung et al., 2021) and mid-Holocene (6ka; Mackallah et al., 2022) experiments. There are an increasing number of studies which have used this model to assess paleo- and future climates (e.g., King et al., 2024; Rashid, 2022; Yeung et al., 2021; Ziehn et al., 2020), with a focus on SH and Australian climates (e.g., Grose et al., 2020; Saini et al., 2025; Yeung et al., 2024), as well as model evaluations (e.g., Purich & England, 2023; Rashid et al., 2022).

Table 1
Orbital Parameters and Greenhouse Gas Concentrations for the piControl, 9 and 8.5 ka Experiments

	piControl	9 ka	8.5 ka
Orbital parameters			
Eccentricity	0.016710222	0.019280	0.019199
Obliquity	23.4393°	24.229°	24.222°
Perihelion-180°	102.94719°	311.26°	319.495°
Date of vernal equinox	March 21 at noon	March 21 at noon	March 21 at noon
Time of perihelion passage in days	2.667	209.58	218.05
Greenhouse gases			
CO_2 (ppm)	284.3	261.3	260
CH_4 (ppb)	808.2	688.1	660
N_2O (ppb)	273.0	261.8	260

Note. The table only display the changing elements in the boundary conditions, all the other forcings for the 9 and 8.5 ka simulations remain the same as piControl. The values for the 9 and 8.5 ka experiments are from Paleoclimate Modelling Intercomparison Project phase 4 transient deglaciation experimental design and Paleoclimate Modelling Intercomparison Project phase 3 experimental design, respectively (https://pmip4.lsce.ipsl.fr/doku.php/exp_design:degla; https://wiki.lsce.ipsl.fr/pmip3/doku.php/pmip3:design:8k2:index#ka_experimental_design).

2.2. Experimental Setup

2.2.1. Background State

We first conducted a 9 ka simulation prior to the 8.2 ka simulation to produce a stable early Holocene background climate state before the abrupt event. The 9 ka simulation was initialized from an official ACCESS-ESM1.5 CMIP6 pre-industrial control experiment (piControl, see Ziehn et al., 2020), forced with orbital parameters and greenhouse gas (GHG) concentrations for 9,000 years BP, and run for 300 model years. The boundary conditions for the early Holocene compared with the piControl experiment are shown in Table 1, with the model configuration and all other forcings remaining the same as the ACCESS-ESM1.5 piControl experiment (see details in Ziehn et al., 2020). Note that the sea level was set to pre-industrial conditions for the 9 ka simulation, similar to the PMIP4 mid-Holocene (6 ka) experiment (Mackallah et al., 2022), and Renssen et al. (2005), who performed a transient experiment of the past 9,000 years. During the last 100 years of spin-up, the experiment displays relatively small trends in global average sea-surface temperature, full-depth ocean temperature and salinity (Figure S1 in Supporting Information S1), reaching an acceptable near-equilibrium state consistent with PMIP protocols and other modeling studies (e.g., Kageyama et al., 2018; Menary et al., 2018; Williams et al., 2020; Yeung et al., 2021).

For the 8.2 ka experiment, we used 8.5 ka boundary conditions for orbital parameters and GHG concentrations, using PMIP3 datasets for consistency with previous studies (see Table 1, same as in Morrill, LeGrande et al., 2013; Renssen et al., 2001, 2002; Wagner et al., 2013). The experiment started from 9 ka equilibrium conditions and the model was run for 50 model years to adapt to the new 8.5 ka boundary conditions, noting that the differences in orbital and GHG concentrations between 9 and 8.5 ka are small (Table 1).

Figure 2 shows the monthly incoming shortwave radiation (SW) at the top of the atmosphere (TOA) at 8.5 ka compared with piControl as a result of the astronomical changes. In the NH, summer (June, July, August, or JJA) insolation is increased by up to 40.7 W/m^2 at 65°N and winter (December, January, February, or DJF) insolation is reduced by up to −2.8 W/m^2 at 65°N. Austral summer (DJF) experienced lower insolation by up to 32.9 W/m^2 while insolation was greater by up to 30.7 W/m^2 at 25°S in late austral winter (JJA) and spring. This results in warmer NH summers (Figure S2c in Supporting Information S1) and cooler winters (Figure S2b in Supporting Information S1). Since austral summer (DJF) received a lower insolation relative to present at 8.5 ka, this leads to a general cooling in the SH (Figure S2b in Supporting Information S1).

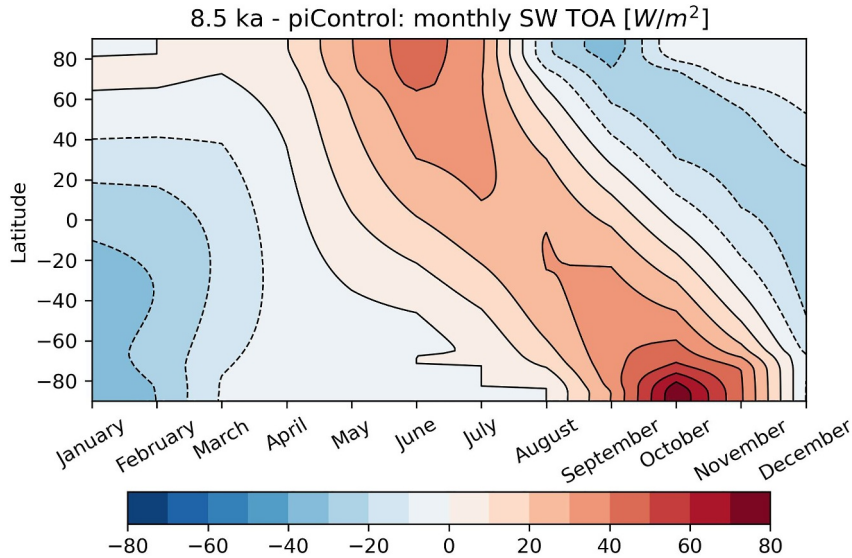

Figure 2. Zonally averaged monthly 8.5 ka—piControl incoming shortwave (SW) net radiation changes (W/m^2) at the top of the atmosphere without calendar adjustment.

2.2.2. Freshwater Forcing Experiments

The North Atlantic meltwater experiments start from the equilibrated 8.5 ka conditions at model year 50 (Figure S3c in Supporting Information S1). The FWF was added following the same approach as previous studies (e.g., PMIP3; Morrill, LeGrande et al., 2013; Wagner et al., 2013; Matero et al., 2017), with a 0.05 Sv background freshwater flux in the Labrador Sea (45–70°N, 50–70°W) to simulate the small continuous flux of meltwater from the Hudson Bay prior to the lake outburst (Carlson et al., 2009). We next completed five idealized FWF experiments to test both the model response to Lake Agassiz drainage and the hypothesis of "lake + saddle collapse" for the cause of the 8.2 ka event (see Table 2) by also adding meltwater in the Labrador Sea.

After 50 years of equilibrating to the new boundary conditions at 8.5 ka, the background flux of 0.05 Sv in the control simulation was run for 200 years (Figure S3c in Supporting Information S1), with the last 70 years considered as the equilibrium state (hereafter referred to as the "control state"). After the 200 year control simulation, the background flux was stopped and four short-duration FWF simulations were performed at model year 250 (Figure S3c in Supporting Information S1): a 1 year pulse of 1 Sv (1Sv_1yr); a 1 year release of the same input volume (1Sv_5yr); 0.5 Sv for 1 years (0.5Sv_5yr), that is equivalent to the "lake outburst" simulation of 2.5 Sv for 1 year as described in the PMIP protocol (Clarke et al., 2004). For comparison, we ran another experiment (1Sv_5yr-re) with the same pulse as 1Sv_5yr, but that started six model years later, with a higher initial AMOC strength than all the other experiments (see Table 2). This experiment was performed to test the model's response to different AMOC initial conditions. After the hosing, these experiments are then continued for a total of 100 years with the 0.05 Sv background meltwater input applied as in the control simulation.

Table 2
Freshwater Forcing Experiments Performed Under 8.5 ka Boundary Conditions With the ACCESS-ESM1.5

Simulation name	Forcing strength (Sv)	Forcing length (yr)	Total run length (yr)	Total equivalent sea-level rise (m)	Initial AMOC strength (Sv)
Control	0.05 Sv	200	200	0.88	20.94
1Sv_1yr	1	1	100	0.52	18.27
1Sv_5yr	1	5	100	0.86	
0.5Sv_5yr	0.5	5	100	0.64	
1Sv_5yr-re	1	5	100	0.86	19.10
FW100yr	0.05–1	100	250	5.92	18.27

A 100 year time-varying forcing experiment (FW100yr) is also included to mimic the long-term meltwater from the saddle collapse accompanied with a lake outburst. The forcing in FW100yr increases linearly by 0.2 Sv per decade and stays at the peak value of 1 Sv for 20 years, followed by the same linear decrease back to the control value (0.05 Sv) (see Figure S3c in Supporting Information S1 for illustration). The experiment is then continued for another 150 years with the 0.05 Sv background flux to monitor the recovery. Although the resulting global mean sea-level rise in FW100yr (see Table 2) is much higher than other modeling and paleo-data estimates of 0.8–2.2 m (e.g., Gregoire et al., 2012; Li et al., 2012; Törnqvist & Hijma, 2012), we included it as an extreme case to test the model sensitivity to freshwater perturbations as well as its climate impacts.

3. Results

3.1. AMOC Response

All experiments simulate a slight 1.1 Sv increase in AMOC strength for 5 years before beginning to decrease due to internal variability of the AMOC on decadal timescale, and the simulated AMOC does not decrease significantly in 1Sv_1yr and 0.5Sv_5yr (Figure 3a). The addition of 1 Sv of freshwater for 5 years in the 1Sv_5yr and 1Sv_5yr-re experiments produce a fast, and slightly significant AMOC reduction by up to 24% from the control mean of 21.6 ± 1.6 Sv. The AMOC strength weakens by up to 5.1 Sv around 20 years after the introduction of the freshwater pulse in 1Sv_5yr and takes another 20 years to recover (Figure 3a). The AMOC response in 1Sv_5yr-re displays a more variable recovery compared with 1Sv_5yr with the same duration of and same influx at a higher initial AMOC strength. A slightly smaller AMOC reduction (4.1 Sv) is simulated, but with a sharper weakening and longer AMOC increase of 7 years in its first response. The AMOC strength then reaches its peak reduction in 10 years and remains at its minimum for six more years before recovering to a higher value after 20 years.

Only in the FW100yr experiment, does the AMOC show a significant reduction without collapsing (up to 62% decrease) that lasts more than 160 years, which matches the duration of 8.2 ka event anomalies in proxy-records (Thomas et al., 2007) as well as the magnitude of weakening obtained in previous modeling studies (e.g., Aguiar et al., 2021; Matero et al., 2017; Wagner et al., 2013). In agreement with previous modeling studies (e.g., Matero et al., 2017; Morrill, LeGrande et al., 2013; Wagner et al., 2013), our results suggest that a single, short-duration (≤5 years) pulse of meltwater (i.e., Lake Agassiz drainage simulations) does not have the capacity to keep the AMOC weakened for ∼160 years in this model.

3.2. Temperature Response

North Atlantic Surface air temperature decreases significantly in 1Sv_5yr, 1Sv_5yr-re and FW100yr experiments (Figure 3b). However, only the weakening in FW100yr is large enough to result in a significant warming in the South Atlantic. The 1Sv_5yr experiment displays a cooling of 1.3°C in the North Atlantic 4 years after the pulse and remains at its minimum for another 3 years before returning to a higher temperature than control (20.0°C ± 0.2°C) (Figure 3b). The 1Sv_5yr-re experiment shows a similar response, but with a much smaller amplitude of temperature decrease that lasts roughly 10 years (Figure 3b). Temperature response in the South Atlantic is much more diverse among experiments (Figure 3c). All short-duration experiments show a rapid temperature increase of ∼0.3°C in the South Atlantic from the control mean of 16.8°C ± 0.1°C except 1Sv_5yr, which displays a more gradual temperature increase, peaking at 27 years after the pulse. The FW100yr experiment simulates a significant cooling of up to 1.9°C that lasts more than 160 years in the North Atlantic, and a South Atlantic warming of up to 1.2°C for roughly 90 years, peaking 15 years later than the North Atlantic temperature maximum. This may provide evidence of the "bipolar seesaw" mechanism, with out of phase hemispheric temperature changes possibly due to the fast transmission of the AMOC signal to the South Atlantic Ocean through the propagation of Kelvin and Rossby waves (Pontes & Menviel, 2024), consistent with Wiersma and Renssen (2006).

Despite the differences in temperature response through time, the annual mean temperature anomalies in 1Sv_5yr and 1Sv_5yr-re experiments (Figure S4 in Supporting Information S1) show similar patterns at their AMOC minima. The warming near the Arctic region is simulated to be more intense in 1Sv_5yr-re, and is associated with slightly enhanced warming over Eurasia. Both experiments show a significant warming in the South Atlantic tropics as well as some warming north of the Antarctic Circumpolar Current (ACC), and some areas of the South Pacific. Since the FWF is released for such short duration in the 1Sv_5yr and 1Sv_5yr-re experiments, the model response is influenced more by the initial state rather than the magnitude of the FWF. With the same amount of

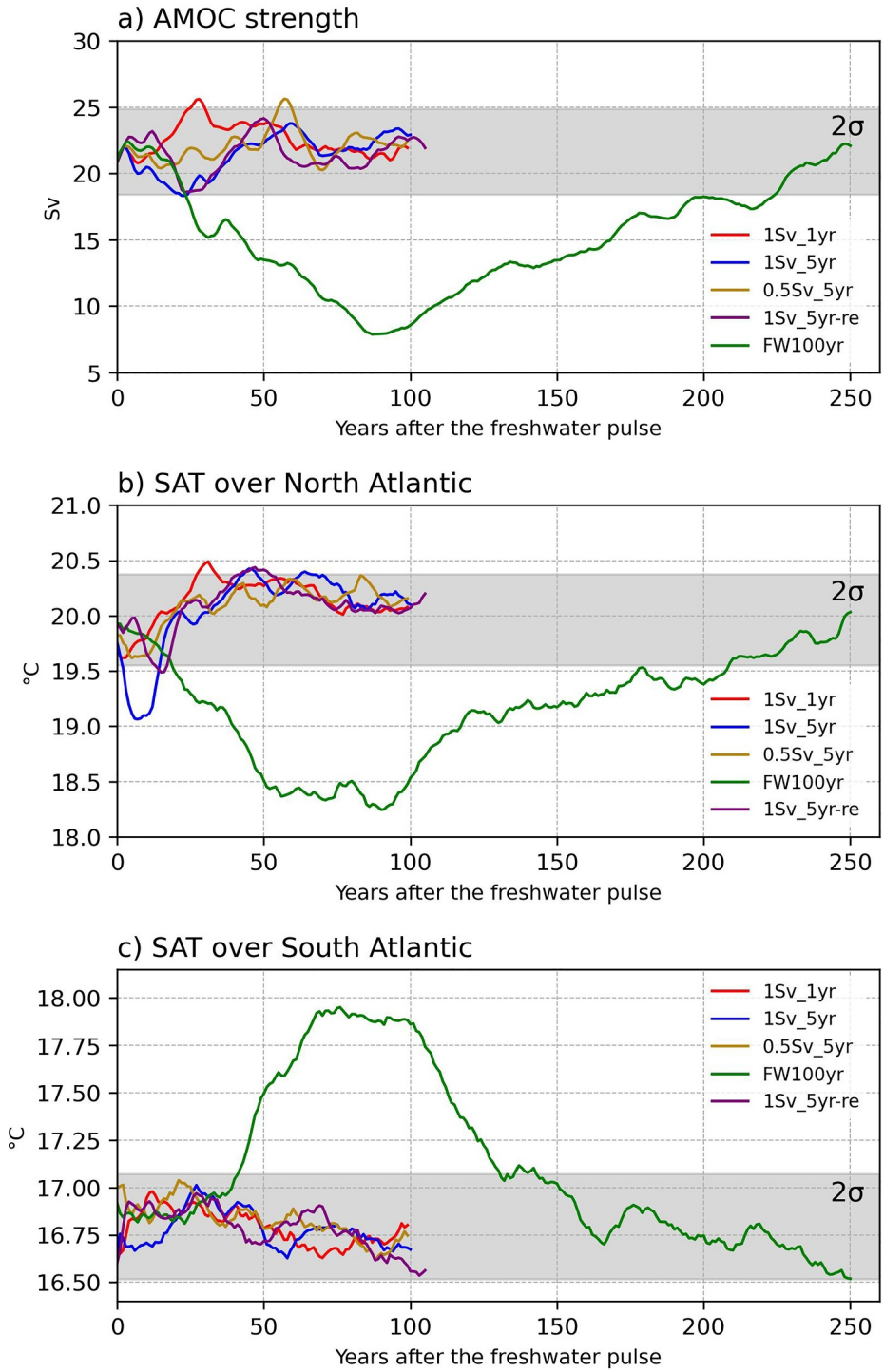

Figure 3. 10 year running mean of (a) maximum strength of the Atlantic Meridional Overturning Circulation (Sv), (b) Surface Air Temperature (SAT; °C) over the North Atlantic (0°N–60°N, 80°W–0°W), (c) SAT (°C) over the South Atlantic (0°S–60°S, 80°W–10°E) since the freshwater forcing at model year 250. The shaded box indicates the two standard deviation (2σ) range of the control variability.

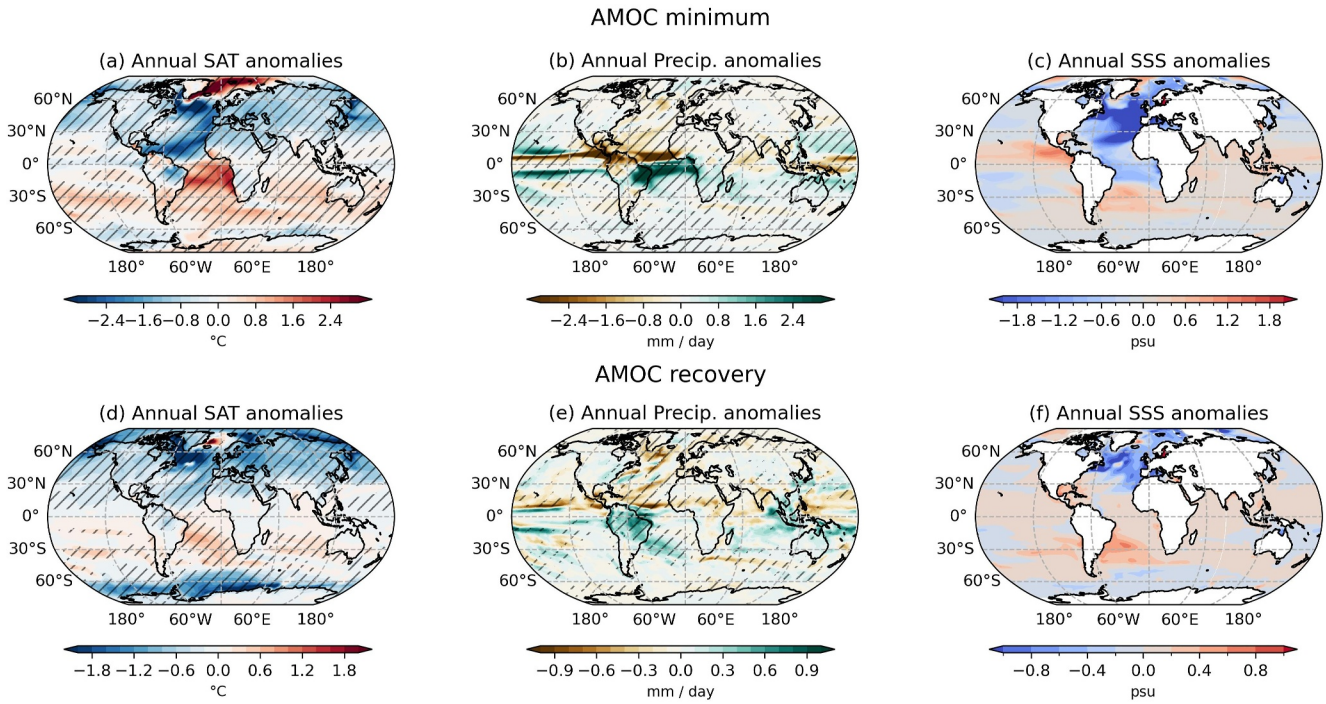

Figure 4. Anomalies of 50 year mean FW100yr minus 70 year mean control (with background fluxes) (a), (d) global annual averaged surface air temperature (°C), (b), (e) annual averaged precipitation (mm/day), and (c), (f) annual sea-surface salinity patterns during Atlantic Meridional Overturning Circulation minimum (top row) and recovery (bottom row). Hachures indicate statically significant differences from the control at the 95% level according to the Student's *t*-test.

input, a larger initial AMOC strength (1Sv_5yr-re) results in quicker and stronger Arctic warming that affects Greenland temperature and parts of NH high latitudes.

Overall, our model simulations with meltwater pulses lasting one to 5 years do not reproduce AMOC and temperature changes of similar magnitude and duration suggested by the 8.2 ka proxy records (Thomas et al., 2007). However, they provide a good indication of model behavior in response to different freshwater perturbations in the North Atlantic under the current interglacial period. In the following part of the paper, we will only use the FW100yr simulation to examine the climate response globally and over Australia. The modeling results are compared with proxy data in the discussion.

3.3. Climatic Response to AMOC Slowdown in FW100yr Experiment

3.3.1. Transient Global Response

First, we analyze the 50 year running mean global climatic response during the AMOC minimum (taken here as the AMOC value below 12 Sv, model years 68–118; see in Figure 3a) and recovery period (years 130–180 in Figure 3a; 12 years after the end of the AMOC minimum period), to examine the climate response through time.

A significant decrease in sea-surface salinity (SSS) is simulated across the North Atlantic during AMOC minimum (Figure 4c), with up to 7.7 psu decrease around the main deep-water formation sites south of Iceland, and between the Greenland and Norwegian Seas (see Figure S5a in Supporting Information S1). During the AMOC recovery period (Figure 4f), this SSS reduction is largely weakened and accompanied by smaller Arctic warming. The mixed layer depth (MLD) is much shallower during AMOC minimum (Figure S5b in Supporting Information S1), associated with the weakening of the AMOC, while the MLD of the main deep-water formation sites recovers quickly only 12 years after the minimum (Figure S5c in Supporting Information S1).

There are some warming anomalies over Greenland during AMOC minimum, but this is followed by significant cooling along with the dissipation of the Arctic warming during recovery (Figures 4a and 4d). Europe (35°N–60°N, 0°E–65°E) temperature is an average of −1.1°C colder relative to control during the AMOC minimum, and −0.9°C colder than control during the recovery phase. The most pronounced temperature changes occur over the

Atlantic Ocean, with maximum NH cooling of up to −5.6°C in the North Atlantic (Figure 4a). The NH (0°N–60°N) experiences an annual mean temperature decrease of −0.7°C during AMOC minimum (Figure 4a), and the significant cooling remains during recovery (Figure 4d). Temperature in the South Atlantic is simulated to be warmed by a maximum of up to 2.6°C, with an SH (0°S–60°S) average warming of 0.3°C compared with the control (Figure 4a). Widespread warming anomalies are simulated in the SH, further suggesting a temperature bipolar see-saw response during AMOC minimum at 8.2 ka. The SH warming is greatly reduced during recovery (Figure 4d). Significant cooling anomalies are simulated over the SH subpolar regions, including intensive cooling in the ACC.

Precipitation changes during AMOC minimum suggests a southward shift in the mean ITCZ position, with reduced precipitation to the North and enhanced precipitation to the south of the equator (Figure 4b). The precipitation rate in the NH tropics (0°N–10°N) is significantly reduced by a mean of −1.6 mm/day, with a maximum decrease of −6.0 mm/day, while precipitation in the SH tropics (0°S–10°S) is significantly enhanced by a mean of 2.8 mm/day, with a maximum increase of up to 5.7 mm/day. The significant precipitation increase in the SH tropics during the AMOC minimum dissipates completely during the recovery phase, potentially indicating a recovery of the ITCZ (Figure 4e).

3.3.2. ITCZ and Monsoon Changes

The previous section gives an overview of the global transient climate response in the FW100yr experiment to understand potential climatic impacts through time due to AMOC weakening in the North Atlantic. Next, we investigate the large-scale climate features (ITCZ and monsoon changes) that may be related to Australian precipitation anomalies during the AMOC minimum period, which shows more consistence with NH temperature proxies, to explore the hydroclimatic response over the SH and Australia during AMOC weakening.

The ITCZ can be identified as the location in the tropical region with maximum precipitation rate, associated with the ascending branch of the Hadley Cell (P. X. Wang et al., 2014). The mean position of the ITCZ is located north of the equator in present-day climate. However, the position can migrate meridionally toward the warmer hemisphere, which is primarily controlled by the AMOC heat transport (Schneider et al., 2014). A southward shift of the ITCZ is typically simulated in climate models with a weakened AMOC (e.g., Chiang & Friedman, 2012; Menviel et al., 2020, Yeung et al., 2021; Saini et al., 2025), this is also seen in our simulations with a significant precipitation decrease in the northern tropics and precipitation increase in the southern tropics in the Atlantic sector during the AMOC minimum (Figure 4b). Below, we further investigate the changes in ITCZ positions during AMOC minimum in each ocean basin.

The global peak precipitation in DJF increases by 22.3% at 7.5°S during the AMOC minimum, while it decreases by 27.7% at 7.5°N in JJA (Figures 5e and 5j). The Atlantic Ocean experiences the most pronounced changes in both seasons (Figures 5d and 5i). In DJF, the control state simulates a double peak both to the north and south of the tropics, the peak increases by up to 64.1% and shifts southwards during the AMOC minimum (Figure 5d). The maximum precipitation over the Atlantic Ocean in JJA experiences a 5° southward shift and a weakening of 15.1% in response to the AMOC minimum (Figure 5i).

The Pacific Ocean is divided into western (130°E−160°W) and eastern sectors (160°W–90°W) to better understand the changes across the basin. The western Pacific simulates a southward shift of 1.25° and slight strengthening in the SH branch (~5°S) of the ITCZ in DJF, whereas the maximum precipitation rate around 5°N in JJA shifts northwards and weakens by 19.6%. On the contrary, the eastern Pacific sector simulates a weakened ITCZ in both seasons, with a northward shift in DJF and southward shift in JJA. A change in the Indian Ocean is less evident in our simulations.

In summary, the ITCZ strengthens and shifts southward over the Atlantic and Western Pacific Oceans in DJF during the AMOC minimum, relative to the control. In JJA, the ITCZ weakens across all ocean basins and only migrates southwards in the Atlantic and Eastern Pacific sectors.

Precipitation anomalies in low latitudes are often associated with changes in large-scale atmospheric circulation, such as displacement of monsoon systems. Here, we investigate precipitation changes in each monsoon domain.

The monsoon domains are defined as regions in which the wet monsoon season precipitation rate exceeds the dry season rate by at least 2.5 mm/day, and is responsible for at least 55% of the annual precipitation (B. Wang et al.,

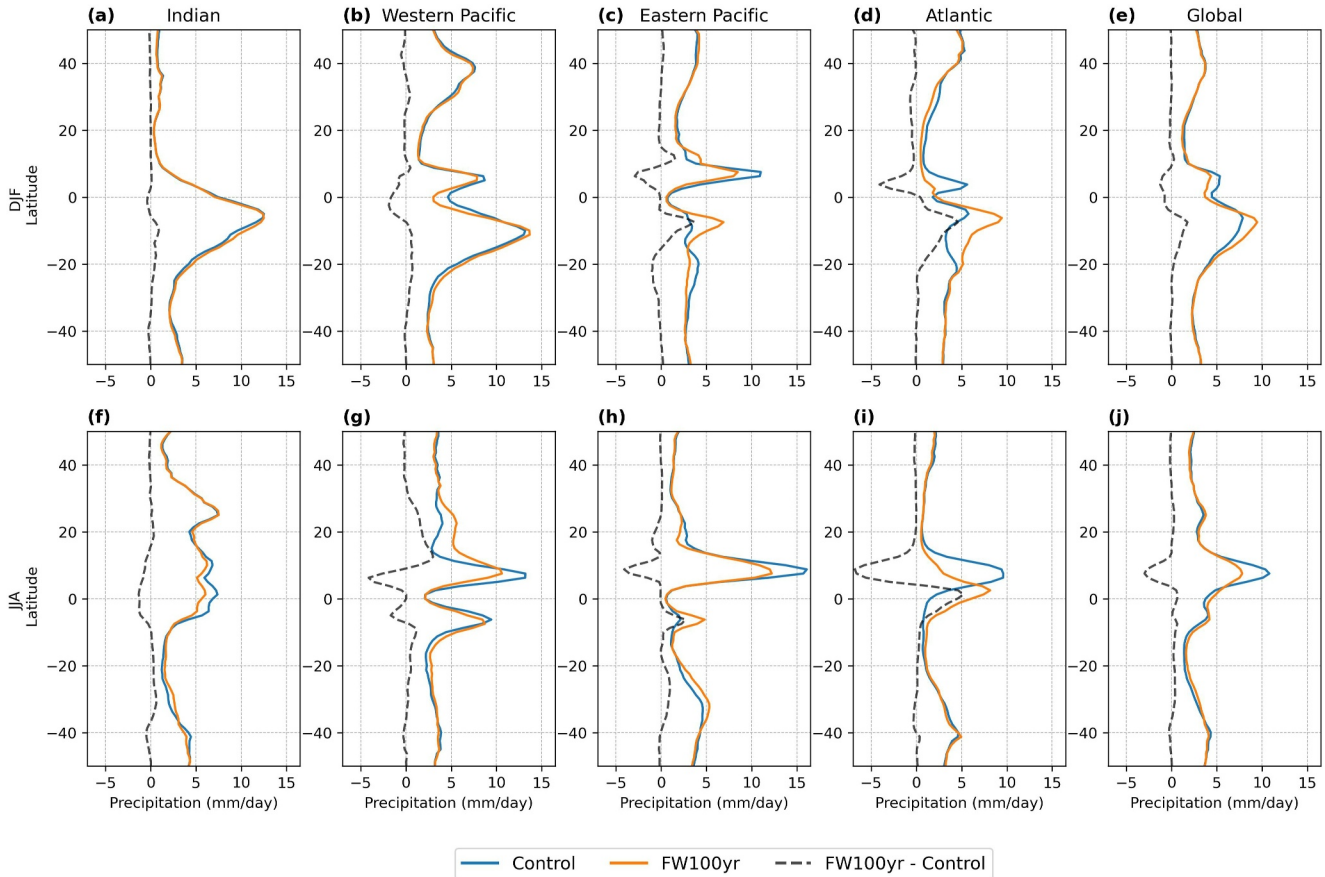

Figure 5. Zonally averaged precipitation (mm/day) in the control and FW100yr (Atlantic Meridional Overturning Circulation minimum) experiments. Indian Ocean is 30°E–110°E; 130°E−160°W covers the Western Pacific Ocean, 160°W–90°W covers the Eastern Pacific Ocean, and 60°W–0°W covers the Atlantic Ocean (a–e) December, January, February (DJF), and (f–j) June, July, August (JJA).

2011; Yeung et al., 2021). The NH monsoon season occurs from May to September (MJJAS), and the dry season occurs from November to March (NDJFM). It is reversed for the SH, with NDJFM being the wet monsoon season, while MJJAS is the dry season.

In the 8.5 ka control state with background fluxes (blue contours in Figure S6 in Supporting Information S1), there is an expansion of the South Asian monsoon, the West African summer monsoon, the western part of the South American monsoon, as well as the SH African monsoon, extending to the Indian Ocean, and the Australian monsoon compared with piControl. In the FW100yr simulation as a result of a weakened AMOC (red contours in Figure 6), a generally contracted summer monsoon domain is simulated over the NH with reduced precipitation (Figure 6a), while a slightly expanded (mainly in the Indo-Australian monsoon region) and stronger SH summer monsoon domain is simulated (Figure 6b).

In MJJAS (Figure 6a), both the South Asian (Indian) summer monsoon and the East Asian summer monsoon are slightly weakened with a more restricted domain. The average precipitation decreases by roughly 18.5% and 6.9%, respectively. The West African summer monsoon is also displaced southwards. In the SH monsoon season (NDJFM; Figure 6b), the Indo-Australian summer monsoon (IASM) is expanded by ∼24.8% over northern Australia with an average precipitation increase of ∼16.3% across the SH tropics in the Indian Ocean and Southwest Pacific domains. The South Pacific Convergence Zone is also displaced to the south. The South American monsoon shows a southward shift with a precipitation increase of up to 6.8 mm/day over the eastern side.

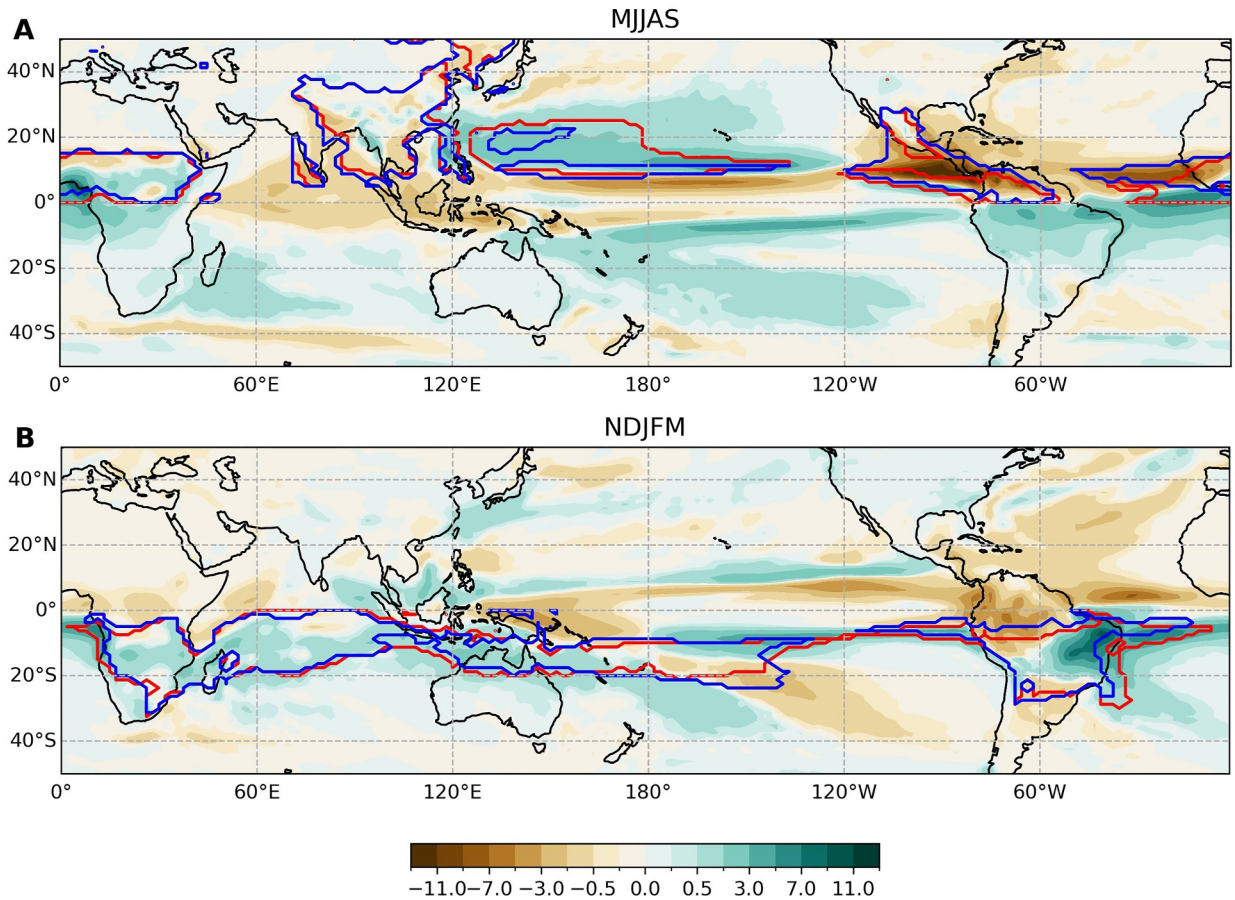

Figure 6. FW100yr (Atlantic Meridional Overturning Circulation minimum)—control precipitation anomaly (mm/day) in (a) Northern Hemisphere monsoon season: MJJAS, and (b) Southern Hemisphere monsoon season: NDJFM. Contours indicate monsoon domains for FW100yr (in red) and for control (in blue) experiments.

3.3.3. Australasian Climate Variability

The annual surface air temperature over the Australian continent (10°S–45°S, 110°E−160°E) increases by a mean of 0.3°C in response to a weakened AMOC (Figure 7a). A cooling of 0.2°C is simulated over Northern Australia (10°S–25°S), associated with increased precipitation, while the southern part of the continent experiences warmer (by 0.4°C) and drier conditions at 8.2 ka during the AMOC minimum (Figures 7a and 7d). This is different from previous studies which show non-significant climate response over the Australian region (e.g., Matero et al., 2017; Morrill et al., 2014; Shi et al., 2020). Australian hydroclimate is influenced by different climate regimes in austral summer (DJF) and winter (JJA) seasons; therefore, our analysis focuses on DJF and JJA seasonal average climates.

In the present-day climate, the active IASM during DJF transports moisture toward northern Australia by the north-westerly winds. A weakened IASM with reduced precipitation is simulated in the 8.5 ka control climate (with background fluxes) compared with PI (Figure S6 in Supporting Information S1). This is due to decreased SH summer insolation in the early Holocene. In response to a weakened AMOC, a slight enhancement and southward migration of the ITCZ in the Western Pacific in DJF (Figure 5b) drives the enhancement and expansion of the IASM (Figure 6b). As a result, a significant DJF precipitation increase of up to 1.6 mm/day is simulated over northern Australia and New Guinea (Figure 7e). The wind patterns and wind divergence at 850 hPa in DJF show consistent changes with precipitation anomalies over the monsoon region, with positive anomalies of low-level wind divergence (orange colors in Figure 7h) coinciding with precipitation reductions (Figure 7e). Areas of increased precipitation are associated with negative divergence anomalies or increased low-level convergence (violet colors) leading to enhanced deep convection and moisture convergence.

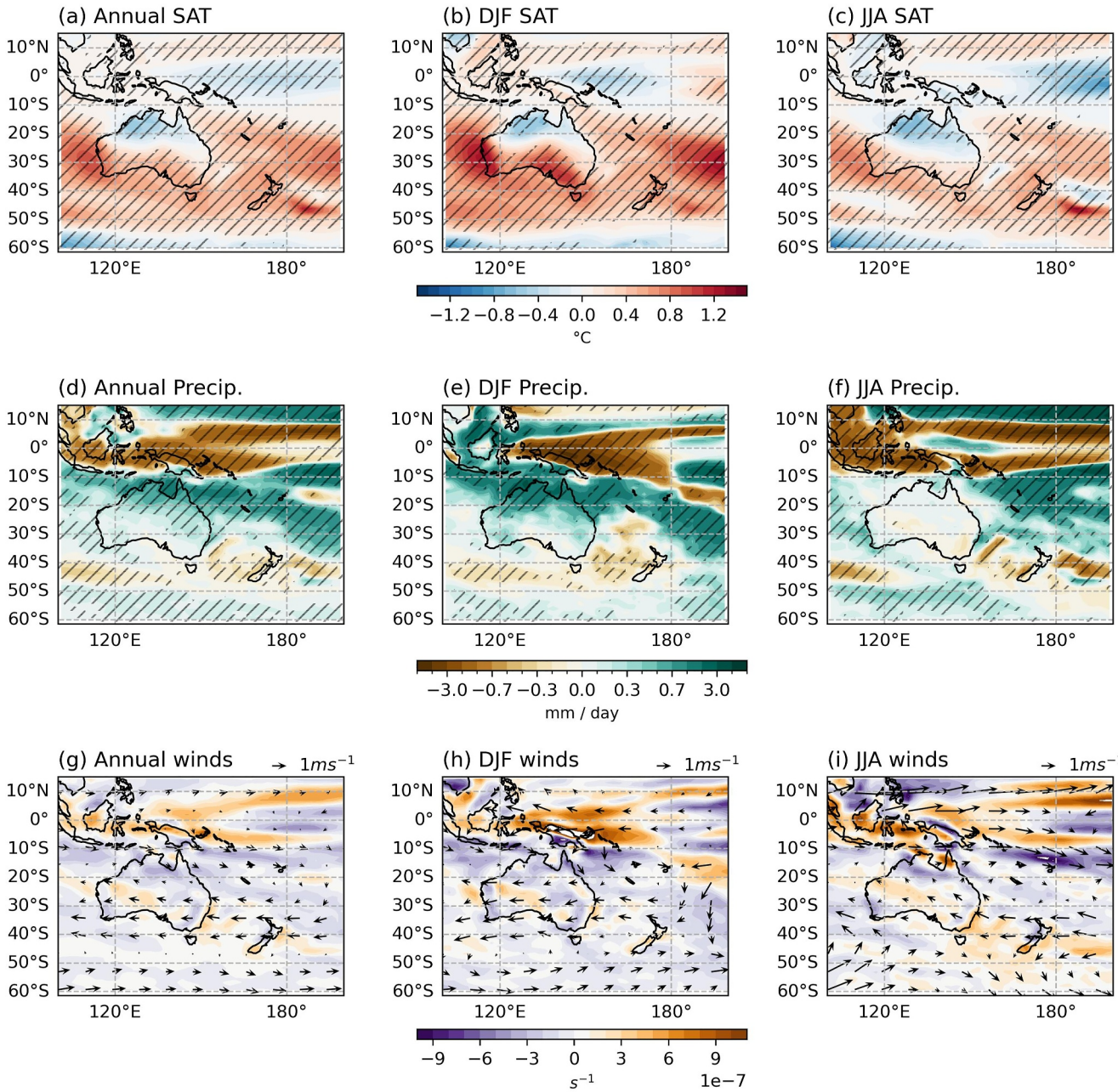

Figure 7. Anomalies FW100yr (Atlantic Meridional Overturning Circulation minimum)—control (with background fluxes) average surface air temperature (°C; top row), precipitation (mm/day; middle row), and 850 hPa winds (m/s) and wind divergence (s^{-1}) (bottom row) over the Australian region for (left) the annual mean, (middle) December, January, February (DJF), and (right) June, July, August (JJA). Hachures indicate statically significant differences from the control at the 95% level according to the Student's *t*-test.

In JJA season in the modern climate, the SH mid-latitude westerlies shift northwards, bringing moisture to the southern Australian continent. In our AMOC minimum experiment, a slight weakening (<1 m/s) of the westerly winds is simulated over the southern Australian continent and offshore regions (Figure 7i). This is associated with non-significant precipitation changes in southern Australia (Figure 7f).

In summary, the surface air temperature displays a similar response to weakened AMOC at 8.2 ka annually and in both seasons, with significant cooling over the northern part, and warmer conditions to the south and also over New Zealand (Figures 7a–7c). Precipitation response over Australia is greatly influenced by the changes in

seasonal atmospheric circulations due to AMOC variability. However, the southern Australian region and New Zealand are likely to be less affected and display drier conditions at all times (Figures 7d–7f).

4. Discussion

4.1. Evaluation of Model Simulations of AMOC Sensitivity at 8.2 ka

This study has evaluated the AMOC response to different idealized freshwater hosing experiments in the North Atlantic in the ACCESS-ESM1.5 model. Of the four short-duration (1–5 years) and one long-term meltwater addition experiments, only the FW100yr experiment with long-term release is able to simulate a sustained >100 years AMOC weakening, which is in agreement with other modeling studies for this event (e.g., LeGrande & Schmidt, 2008; Matero et al., 2017; Morrill, LeGrande et al., 2013; Wagner et al., 2013). This also supports the idea proposed in previous modeling studies (e.g., Gregoire et al., 2012; Matero et al., 2017) that a "lake + ice collapse" pulse is more likely to explain the two-stage anomalies in proxy records (Rohling & Pälike, 2005). Short meltwater pulse experiments starting at different initial AMOC strength (1Sv_5yr and 1Sv_5yr_re) both lead to a similar AMOC weakening and climate response even though the warming anomalies in the North Atlantic and Arctic regions are much larger in the 1Sv_5yr_re experiment. Future research should aim to conduct more experiments starting from various initial conditions to further validate this proposition.

Our results also suggest that the FWF release duration influences the AMOC response in this model. A 1-year pulse does not produce any significant changes in the AMOC compared with the same volume of input for 5 years. The signal starts to appear after 5 years in our model and is likely to keep increasing as additional FWF is added over a longer time. However, from our control experiment of a 200 year input of 0.05 Sv (starting at year 50), the impact on AMOC is still insignificant (Figure S3a in Supporting Information S1), since it requires ∼0.4 Sv to shut down the AMOC in this model (Saini et al., 2025). In addition, neither our 5-year freshwater perturbation of "lake outburst" simulation (0.5Sv_5yr) equivalent to the PMIP protocols (Clarke et al., 2004), nor the 1Sv_5yr and 1Sv_5yr-re experiments of total sea-level rise consistent with the latest estimates (Li et al., 2012) lead to significant changes in AMOC. Although further validation in more hosing experiments is needed, this suggests that the AMOC response in this model is sensitive to both the rate and duration of freshwater pulses, future studies should carefully consider both criteria when simulating this event.

The model simulates an unexpected Arctic warming in all FWF experiments (e.g., Figure 4 and Figure S4 in Supporting Information S1). Even in our simulation of AMOC duration changes best matched with the proxies, the simulated Greenland temperature does not significantly decrease as suggested in the ice core records. Moreover, from the comparison of our two 1Sv_5yr experiments at the same AMOC minimum period (Figure S4 in Supporting Information S1), we can see that Arctic warming is likely to be magnified in the 1Sv_5yr-re experiment, which starts at a higher initial AMOC strength. Similar North Atlantic subpolar warming patterns are also seen in the FWF experiments performed under early Holocene climates using the AWI-ESM model using different model resolutions (Shi et al., 2020), where they suggest that the subpolar warming is less intense in lower-resolution models. Possible causes can be related to changes in zonal density gradient due to the meltwater input, which affect the circulation in the subpolar Atlantic region thus leading to a transient polar warming (e.g., Born & Levermann, 2010). However, further investigation is needed for the observed response in the ACCESS-ESM1.5 model.

4.2. Model-Data Comparison

Fourteen out of 32 sites in the SH summarized in Table S1 and S2 in Supporting Information S1 show no distinct signals during the 8.2 ka event. There are many reasons why certain time series or regions may show no response. These include: the region did not respond to the climate trigger; competing environmental processes cancel out changes in a proxy signal at a site (particularly relevant for speleothems $\delta^{18}O$); climate proxies are not sensitive enough to record the local climate shift (complacency); and insufficient age control or resolution (Parker & Harrison, 2022). Where model output contradicts the 8.2 ka signal in the proxy data, this could be either a modeling problem or proxy interpretation problem.

Due to limited temperature signals in the SH proxy records, it is unclear whether a bipolar seesaw response was established during the 8.2 ka event. In our FW100yr experiment, widespread SH warming is simulated during both the AMOC minimum and the recovery phase (Figures 4a and 4d) with a 15 year lag between the temperature

peaks in the North and South Atlantic Oceans (Figures 3b and 3c), suggesting a bipolar seesaw response. Proxy reconstructions indicate a widespread cooling of ~1°C–1.5°C over Europe (as syntheses in Morrill, Anderson, et al., 2013; Parker & Harrison, 2022), and up to 3.3°C cooling from Greenland ice cores (Kobashi et al., 2007). The magnitude of cooling across Europe is more consistent with our FW100yr simulation during the AMOC minimum period, when the model simulated a 1.1°C mean cooling compared with the recovery phase when the model simulated only 0.9°C cooling (as mentioned in Section 3.3.1). However, the FW100yr simulation does not reproduce the reconstructed cooling over Greenland due to the Arctic warming in the model. Therefore, we compare proxy records to our AMOC minimum period (model years 68–118 in Figure 3a) in the FW100yr experiment which shows more consistent with NH temperature anomalies during the 8.2 ka event.

Our simulation of precipitation patterns during AMOC minimum is overall consistent with the synthesis from Morrill, Anderson, et al. (2013), with decreased precipitation in Greenland, Asia, southern Europe, central America and New Zealand as well as enhanced precipitation in SH tropics. A southward shift of the ITCZ at 8.2 ka is suggested in multiple paleoclimate records and model simulations (e.g., Parker & Harrison, 2022; Tindall & Valdes, 2011; Wiersma & Renssen, 2006) although a speleothem record from northwest Australia does not show a clear 8.2 ka signal (Denniston et al., 2013). In this study, our model simulations support a southward shift of the ITCZ over the Western Pacific Ocean during the monsoon season (DJF), as well as displaying a significant precipitation increase in the Indo-Australian monsoon region during AMOC minimum. This is in contrast with previous model simulations which did not find a significant change in Indo-Australian monsoon precipitation (e.g., Morrill et al., 2014; Wagner et al., 2013). The model also simulates a weakened Indian and East Asian monsoon during AMOC minimum (Figure 6a), which is consistent with the high-resolution stalagmite oxygen isotope records from southern Oman (Fleitmann et al., 2003), Dongge Cave in southern China (Y. Wang et al., 2005), and high-resolution speleothem record in northern Laos (Wood et al., 2023). The South American monsoon is simulated to shift southward with a precipitation increase of up to 6.8 mm/day over the eastern sector during AMOC minimum (Figure 6b). This is consistent with speleothem records from the region and simulations using CCSM3 and UVic models (Aguiar et al., 2020). A slight weakening of the SH westerlies over southern Australia is simulated in JJA, which is partly consistent with a synthesis of high-resolution Holocene proxies (De Deckker, 2022).

5. Conclusions

This study presents an analysis of the potential impacts of an AMOC weakening on the SH and Australian regions in an idealized 8.2 ka freshwater hosing simulation using the ACCESS-ESM1.5 model. While the largest changes are simulated in the Atlantic Ocean region, Australian climate is found to be more directly influenced by a southward shift in the mean DJF position of the Pacific ITCZ, and consequently an enhanced IASM. During the 8.2 ka AMOC minimum, cooler and wetter conditions are simulated over northern Australia, while there is warming and slightly reduced precipitation over southern Australia with weakened SH westerlies in JJA. The results provide new insights into the regional climate response over Australia from the ACCESS-ESM1.5 model which had demonstrated high skill in simulating the SH and Australian climates (Grose et al., 2020; Ziehn et al., 2020). Sensitivity tests of model AMOC response to FWF in the North Atlantic indicate a long-term freshwater pulse (i.e., "lake + saddle collapse") is more likely to reproduce the reconstructed 8.2 ka cooling over Greenland, supporting previous modeling studies (e.g., Matero et al., 2017).

Although the FW100yr experiment designed for the "lake + saddle collapse" simulation in this study is highly idealized, the duration and magnitude of AMOC weakening are consistent with proxies and previous modeling studies (e.g., Aguiar et al., 2021; Matero et al., 2017; Thomas et al., 2007; Wagner et al., 2013). Simulated regional NH climate anomalies are broadly consistent with proxy records for the 8.2 ka event synthesized in Morrill, Anderson, et al. (2013) and Parker and Harrison (2022). The simulation thus presents a plausible experiment in which to examine the SH climate response to the 8.2 ka event. While our simulations are generally consistent with available SH proxy records, the lack of high-resolution records over the Australian region limits model-proxy comparisons.

Analysis of these simulations can assist evaluation of model AMOC processes as well as providing insight into the links between changes in North Atlantic climate and the SH and Australian region. This can be crucial for understanding potential future AMOC impacts in the SH, particularly given that there are some observed changes

in the AMOC already and most of the CMIP5 and CMIP6 future projection scenarios indicate weakened AMOC in the 21st century (Fox-Kemper et al., 2021).

Data Availability Statement

The model outputs are available at (Du et al., 2025).

Acknowledgments

The authors would like to thank Gabriel Pontes and Pauline Treble for their valuable help in this research. Yanxuan Du, Josephine R. Brown, Laurie Menviel, Himadri Saini, and Russell N. Drysdale acknowledge the funding from the Australian Research Council (ARC) Grant DP220102134. Yanxuan Du and Josephine R. Brown have received support from the ARC Centre of Excellence for Climate Extremes (Grant CE170100023). Josephine R. Brown received support from ARC Centre of Excellence for Weather of the 21st Century (CE230100012). Laurie Menviel acknowledge the support from ARC Grant SR200100008. The work was also completed with the assistance of resources from the National Computational Infrastructure (NCI), which is supported by the Australian Government. This research was supported by the Research Computing Services NCI Access scheme at The University of Melbourne. Open access publishing facilitated by The University of Melbourne, as part of the Wiley - The University of Melbourne agreement via the Council of Australian University Librarians.

References

Aguiar, W., Meissner, K. J., Montenegro, A., Prado, L., Wainer, I., Carlson, A. E., & Mata, M. M. (2021). Magnitude of the 8.2 ka event freshwater forcing based on stable isotope modelling and comparison to future Greenland melting. *Scientific Reports*, *11*(1), 1–10. https://doi.org/10.1038/s41598-021-84709-5

Aguiar, W., Prado, L. F., Wainer, I., Liu, Z., Montenegro, A., Meissner, K. J., & Mata, M. M. (2020). Freshwater forcing control on early-Holocene South American monsoon. *Quaternary Science Reviews*, *245*, 106498. https://doi.org/10.1016/j.quascirev.2020.106498

Alley, R. B., Mayewski, P. A., Sowers, T., Stuiver, M., Taylor, K. C., & Clark, P. U. (1997). Holocene climatic instability: A prominent, widespread event 8200 yr ago. *Geology*, *25*(6), 483. https://doi.org/10.1130/0091-7613(1997)025<0483:HCIAPW>2.3.CO;2

Augustinus, P., Bleakley, N., Deng, Y., Shane, P., & Cochran, U. (2008). Rapid change in early Holocene environments inferred from lake Pupuke, Auckland city, New Zealand. *Journal of Quaternary Science*, *23*(5), 435–447. https://doi.org/10.1002/jqs.1153

Azevedo, V., Strikis, N. M., Novello, V. F., Roland, C. L., Cruz, F. W., Santos, R. V., et al. (2021). Paleovegetation seesaw in Brazil since the late Pleistocene: A multiproxy study of two biomes. *Earth and Planetary Science Letters*, *563*, 116880. https://doi.org/10.1016/j.epsl.2021.116880

Bellouin, N., Martin, G. M., Bellouin, N., Collins, W. J., Culverwell, I. D., Halloran, P. R., et al. (2011). The HadGEM2 family of Met Office unified model climate configurations. *Geoscientific Model Development*, *4*(3), 723–757. https://doi.org/10.5194/gmd-4-723-2011

Boch, R., Spötl, C., & Kramers, J. (2009). High-resolution isotope records of early Holocene rapid climate change from two coeval stalagmites of Katerloch Cave, Austria. *Quaternary Science Reviews*, *28*(23–24), 2527–2538. https://doi.org/10.1016/j.quascirev.2009.05.015

Born, A., & Levermann, A. (2010). The 8.2 ka event: Abrupt transition of the subpolar gyre toward a modern North Atlantic circulation. *Geochemistry, Geophysics, Geosystems*, *11*(6). https://doi.org/10.1029/2009GC003024

Buckley, M. W., & Marshall, J. (2016). Observations, inferences, and mechanisms of the Atlantic meridional overturning circulation: A review. *Reviews of Geophysics*, *54*(1), 5–63. https://doi.org/10.1002/2015RG000493

Carlson, A. E., Clark, P. U., Haley, B. A., & Klinkhammer, G. P. (2009). Routing of western Canadian Plains runoff during the 8.2 ka cold event. *Geophysical Research Letters*, *36*(14). https://doi.org/10.1029/2009GL038778

Chiang, J. C. H., & Friedman, A. R. (2012). Extratropical cooling, interhemispheric thermal gradients, and tropical climate change. *Annual Review of Earth and Planetary Sciences*, *40*(1), 383–412. https://doi.org/10.1146/annurev-earth-042711-105545

Clarke, G. K. C., Bush, A. B. G., & Bush, J. W. M. (2009). Freshwater discharge, sediment transport, and modeled climate impacts of the final drainage of glacial Lake Agassiz. *Journal of Climate*, *22*(8), 2161–2180. https://doi.org/10.1175/2008JCLI2439.1

Clarke, G. K. C., Leverington, D. W., Teller, J. T., & Dyke, A. S. (2004). Paleohydraulics of the last outburst flood from glacial Lake Agassiz and the 8200BP cold event. *Quaternary Science Reviews*, *23*(3–4), 389–407. https://doi.org/10.1016/j.quascirev.2003.06.004

Comas-Bru, L., Rehfeld, K., Roesch, C., Amirnezhad-Mozhdehi, S., Harrison, S. P., Atsawawaranunt, K., et al., SISAL Working Group members. (2020). SISALv2: A comprehensive speleothem isotope database with multiple age–depth models. *Earth System Science Data*, *12*(4), 2579–2606. https://doi.org/10.5194/essd-12-2579-2020

De Deckker, P. (2022). The Holocene hypsithermal in the Australian region. *Quaternary Science Advances*, *7*, 100061. https://doi.org/10.1016/j.qsa.2022.100061

Denniston, R. F., Wyrwoll, K.-H., Polyak, V. J., Brown, J. R., Asmerom, Y., Wanamaker, A. D., et al. (2013). A Stalagmite record of Holocene Indonesian–Australian summer monsoon variability from the Australian tropics. *Quaternary Science Reviews*, *78*, 155–168. https://doi.org/10.1016/j.quascirev.2013.08.004

Du, Y., Brown, J. R., Menviel, L., Saini, H., & Drysdale, R. N. (2025). Data from: The impacts of an AMOC slowdown on Southern Hemisphere and Australian climates at 8.2 ka in ACCESS-ESM1.5 model [Dataset]. *Dryad*. https://doi.org/10.5061/dryad.8pk0p2nxj

Eyring, V., Bony, S., Meehl, G. A., Senior, C. A., Stevens, B., Stouffer, R. J., & Taylor, K. E. (2016). Overview of the Coupled Model Intercomparison Project Phase 6 (CMIP6) experimental design and organization. *Geoscientific Model Development*, *9*, 1937–1958. https://doi.org/10.5194/gmd-9-1937-2016

Fleitmann, D., Burns, S. J., Mudelsee, M., Neff, U., Kramers, J., Mangini, A., & Matter, A. (2003). Holocene forcing of the Indian monsoon recorded in a stalagmite from southern Oman. *Science*, *300*(5626), 1737–1739. https://doi.org/10.1126/science.1083130

Fox-Kemper, B., Hewitt, H. T., Xiao, C., Aðalgeirsdóttir, G., Drijfhout, S. S., Edwards, T. L., et al. (2021). Ocean, Cryosphere and Sea Level Change. In V. Masson-Delmotte, P. Zhai, A. Pirani, S. L. Connors, C. Péan, S. Berger, et al. (Eds.), *Climate Change 2021: The Physical Science Basis, Contribution of Working Group I to the Sixth Assessment Report of the Intergovernmental Panel on Climate Change* (pp. 1211–1362). Cambridge, UK: Cambridge University Press. https://doi.org/10.1017/9781009157896.011

Gregoire, L. J., Payne, A. J., & Valdes, P. J. (2012). Deglacial rapid sea level rises caused by ice-sheet saddle collapses. *Nature*, *487*(7406), 219–222. https://doi.org/10.1038/nature11257

Griffies, S. M. (2012). Elements of MOM5. *GFDL Ocean Group Technology*. Rep. No. 7. NOAA/Geophysical Fluid Dynamics Laboratory.

Grose, M. R., Narsey, S., Delage, F. P., Dowdy, A. J., Bador, M., Boschat, G., et al. (2020). Insights from CMIP6 for Australia's future climate. *Earth's Future*, *8*(5), e2019EF001469. https://doi.org/10.1029/2019EF001469

Hoffman, J. S., Carlson, A. E., Winsor, K., Klinkhammer, G. P., LeGrande, A. N., Andrews, J. T., & Strasser, J. C. (2012). Linking the 8.2 ka event and its freshwater forcing in the Labrador Sea. *Geophysical Research Letters*, *39*(18), 2012GL053047. https://doi.org/10.1029/2012GL053047

Hunke, E. C., & Lipscomb, W. H. (2010). *CICE: The Los Alamos sea ice model documentation and software user's manual, Version 4.1, LACC06-012*. Los Alamos National Laboratory.

Kageyama, M., Braconnot, P., Harrison, S. P., Haywood, A. M., Jungclaus, J. H., Otto-Bliesner, B. L., et al. (2018). The PMIP4 contribution to CMIP6 – Part 1: Overview and over-arching analysis plan. *Geoscientific Model Development*, *11*(3), 1033–1057. https://doi.org/10.5194/gmd-11-1033-2018

Kaushal, N., Lechleitner, F. A., Wilhelm, M., Azennoud, K., Bühler, J. C., Braun, K., et al., SISAL Working Group members. (2024). SISALv3: A global speleothem stable isotope and trace element database. *Earth System Science Data*, *16*(4), 1933–1963. https://doi.org/10.5194/essd-16-1933-2024

King, A. D., Ziehn, T., Chamberlain, M., Borowiak, A. R., Brown, J. R., Cassidy, L., et al. (2024). Exploring climate stabilisation at different global warming levels in ACCESS-ESM-1.5. https://doi.org/10.5194/egusphere-2023-2961

Kobashi, T., Severinghaus, J. P., Brook, E. J., Barnola, J.-M., & Grachev, A. M. (2007). Precise timing and characterization of abrupt climate change 8200 years ago from air trapped in polar ice. *Quaternary Science Reviews*, *26*(9–10), 1212–1222. https://doi.org/10.1016/j.quascirev.2007.01.009

Kowalczyk, E., Stevens, L., Law, R., Dix, M., Wang, Y., Harman, I., et al. (2013). The land surface model component of ACCESS: Description and impact on the simulated surface climatology. *Australian Meteorological and Oceanographic Journal*, *63*(1), 65–82. https://doi.org/10.22499/2.6301.005

LeGrande, A. N., & Schmidt, G. A. (2008). Ensemble, water isotope–enabled, coupled general circulation modeling insights into the 8.2 ka event. *Paleoceanography*, *23*(3). https://doi.org/10.1029/2008PA001610

Li, Y.-X., Renssen, H., Wiersma, A. P., & Törnqvist, T. E. (2009). Investigating the impact of Lake Agassiz drainage routes on the 8.2 ka cold event with a climate model. *Climate of the Past*, *5*(3), 471–480. https://doi.org/10.5194/cp-5-471-2009

Li, Y.-X., Törnqvist, T. E., Nevitt, J. M., & Kohl, B. (2012). Synchronizing a sea-level jump, final Lake Agassiz drainage, and abrupt cooling 8200years ago. *Earth and Planetary Science Letters*, *315–316*, 41–50. https://doi.org/10.1016/j.epsl.2011.05.034

Logan, A. J. (2011). *A new paleoclimate record for North Westland, New Zealand, with implications for the interpretation of speleothem based paleoclimate proxies*. (master's thesis). University of Canterbury. Retrived from UC Research. https://doi.org/10.26021/6445

Mackallah, C., Chamberlain, M. A., Law, R. M., Dix, M., Ziehn, T., Bi, D., et al. (2022). ACCESS datasets for CMIP6: Methodology and idealised experiments. *Journal of Southern Hemisphere Earth Systems Science*, *72*(2), 93–116. https://doi.org/10.1071/ES21031

Martin, G. M., Milton, S. F., Senior, C. A., Brooks, M. E., Ineson, S., Reichler, T., & Kim, J. (2010). Analysis and reduction of systematic errors through a seamless approach to modeling weather and climate. *Journal of Climate*, *23*(22), 5933–5957. https://doi.org/10.1175/2010JCLI3541.1

Matero, I. S. O., Gregoire, L. J., Ivanovic, R. F., Tindall, J. C., & Haywood, A. M. (2017). The 8.2 ka cooling event caused by Laurentide ice saddle collapse. *Earth and Planetary Science Letters*, *473*, 205–214. https://doi.org/10.1016/j.epsl.2017.06.011

Menary, M. B., Kuhlbrodt, T., Ridley, J., Andrews, M. B., Dimdore-Miles, O. B., Deshayes, J., et al. (2018). Preindustrial control simulations with HadGEM3-GC3.1 for CMIP6. *Journal of Advances in Modeling Earth Systems*, *10*(12), 3049–3075. https://doi.org/10.1029/2018MS001495

Menviel, L. C., Skinner, L. C., Tarasov, L., & Tzedakis, P. C. (2020). An ice–climate oscillatory framework for Dansgaard–Oeschger cycles. *Nature Reviews Earth and Environment*, *1*(12), 677–693. https://doi.org/10.1038/s43017-020-00106-y

Morrill, C., Anderson, D. M., Bauer, B. A., Buckner, R., Gille, E. P., Gross, W. S., et al. (2013). Proxy benchmarks for intercomparison of 8.2 ka simulations. *Climate of the Past*, *9*(1), 423–432. https://doi.org/10.5194/cp-9-423-2013

Morrill, C., LeGrande, A. N., Renssen, H., Bakker, P., & Otto-Bliesner, B. L. (2013). Model sensitivity to North Atlantic freshwater forcing at 8.2 ka. *Climate of the Past*, *9*(2), 955–968. https://doi.org/10.5194/cp-9-955-2013

Morrill, C., Ward, E. M., Wagner, A. J., Otto-Bliesner, B. L., & Rosenbloom, N. (2014). Large sensitivity to freshwater forcing location in 8.2 ka simulations. *Paleoceanography*, *29*(10), 930–945. https://doi.org/10.1002/2014PA002669

Nicolussi, K., & Schluchter, C. (2012). The 8.2 ka event—Calendar-dated glacier response in the Alps. *Geology*, *40*(9), 819–822. https://doi.org/10.1130/G32406.1

Otto-Bliesner, B. L., Braconnot, P., Harrison, S. P., Lunt, D. J., Abe-Ouchi, A., Albani, S., et al. (2017). The PMIP4 contribution to CMIP6 – Part 2: Two interglacials, scientific objective and experimental design for Holocene and Last Interglacial simulations. *Geoscientific Model Development*, *10*(11), 3979–4003. https://doi.org/10.5194/gmd-10-3979-2017

Parker, S. E., & Harrison, S. P. (2022). The timing, duration and magnitude of the 8.2 ka event in global speleothem records. *Scientific Reports*, *12*(1), 10542. https://doi.org/10.1038/s41598-022-14684-y

Pontes, G. M., & Menviel, L. (2024). Weakening of the Atlantic Meridional Overturning Circulation driven by subarctic freshening since the mid-twentieth century. *Nature Geoscience*, *17*(12), 1291–1298. https://doi.org/10.1038/s41561-024-01568-1

Purich, A., & England, M. H. (2023). Projected impacts of Antarctic meltwater anomalies over the twenty-first century. *Journal of Climate*, *36*(8), 2703–2719. https://doi.org/10.1175/JCLI-D-22-0457.1

Rashid, H. A. (2022). Forced changes in El Niño–Southern Oscillation due to global warming and the associated uncertainties in ACCESS-ESM1.5 large ensembles. *Frontiers in Climate*, *4*, 954449. https://doi.org/10.3389/fclim.2022.954449

Rashid, H. A., Sullivan, A., Dix, M., Bi, D., Mackallah, C., Ziehn, T., et al. (2022). Evaluation of climate variability and change in ACCESS historical simulations for CMIP6. *Journal of Southern Hemisphere Earth Systems Science*, *72*(2), 73–92. https://doi.org/10.1071/ES21028

Renssen, H., Goosse, H., & Fichefet, T. (2002). Modeling the effect of freshwater pulses on the early Holocene climate: The influence of high-frequency climate variability. *Paleoceanography*, *17*(2). https://doi.org/10.1029/2001PA000649

Renssen, H., Goosse, H., Fichefet, T., & Campin, J.-M. (2001). The 8.2 kyr BP event simulated by a global atmosphere—Sea-Ice—Ocean model. *Geophysical Research Letters*, *28*(8), 1567–1570. https://doi.org/10.1029/2000GL012602

Renssen, H., Goosse, H., Fichefet, T., Masson-Delmotte, V., & Koç, N. (2005). Holocene climate evolution in the high-latitude Southern Hemisphere simulated by a coupled atmosphere–sea ice–ocean–vegetation model. *The Holocene*, *15*(7), 951–964. https://doi.org/10.1191/0959683605hl869ra

Rohling, E. J., & Pälike, H. (2005). Centennial-scale climate cooling with a sudden cold event around 8,200 years ago. *Nature*, *434*(7036), 975–979. https://doi.org/10.1038/nature03421

Saini, H., Pontes, G., Brown, J. R., Drysdale, R. N., Du, Y., & Menviel, L. (2025). Australasian hydroclimate response to the collapse of the atlantic meridional overturning circulation under pre-industrial and last interglacial climates. *Paleoceanography and Paleoclimatology*, *40*, e2024PA004967. https://doi.org/10.1029/2024PA004967

Schneider, T., Bischoff, T., & Haug, G. H. (2014). Migrations and dynamics of the intertropical convergence zone. *Nature*, *513*(7516), 45–53. https://doi.org/10.1038/nature13636

Shi, X., Lohmann, G., Sidorenko, D., & Yang, H. (2020). Early-Holocene simulations using different forcings and resolutions in AWI-ESM. *The Holocene*, *30*(7), 996–1015. https://doi.org/10.1177/0959683620908634

Stocker, T. F., & Johnsen, S. J. (2003). A minimum thermodynamic model for the bipolar seesaw. *Paleoceanography*, *18*(4). https://doi.org/10.1029/2003PA000920

Tamhane, J., Thomas, Z. A., Cadd, H., Harris, M. R. P., Turney, C., Marjo, C. E., et al. (2023). Mid-Holocene intensification of Southern Hemisphere westerly winds and implications for regional climate dynamics. *Quaternary Science Reviews*, *305*, 108007. https://doi.org/10.1016/j.quascirev.2023.108007

Teller, J. T., Leverington, D. W., & Mann, J. D. (2002). Freshwater outbursts to the oceans from glacial Lake Agassiz and their role in climate change during the last deglaciation. *Quaternary Science Reviews*, *21*(8–9), 879–887. https://doi.org/10.1016/S0277-3791(01)00145-7

Thomas, E. R., Wolff, E. W., Mulvaney, R., Steffensen, J. P., Johnsen, S. J., Arrowsmith, C., et al. (2007). The 8.2ka event from Greenland ice cores. *Quaternary Science Reviews*, *26*(1–2), 70–81. https://doi.org/10.1016/j.quascirev.2006.07.017

Tindall, J. C., & Valdes, P. J. (2011). Modeling the 8.2ka event using a coupled atmosphere–ocean GCM. *Global and Planetary Change*, *79*(3), 312–321. https://doi.org/10.1016/j.gloplacha.2011.02.004

Törnqvist, T. E., & Hijma, M. P. (2012). Links between early Holocene ice-sheet decay, sea-level rise and abrupt climate change. *Nature Geoscience*, *5*(9), 601–606. https://doi.org/10.1038/ngeo1536

Utida, G., Cruz, F. W., Santos, R. V., Sawakuchi, A. O., Wang, H., Pessenda, L. C. R., et al. (2020). Climate changes in Northeastern Brazil from deglacial to Meghalayan periods and related environmental impacts. *Quaternary Science Reviews*, *250*, 106655. https://doi.org/10.1016/j.quascirev.2020.106655

Vinther, B. M., Clausen, H. B., Johnsen, S. J., Rasmussen, S. O., Andersen, K. K., Buchardt, S. L., et al. (2006). A synchronized dating of three Greenland ice cores throughout the Holocene. *Journal of Geophysical Research*, *111*(D13). https://doi.org/10.1029/2005JD006921

Wagner, A. J., Morrill, C., Otto-Bliesner, B. L., Rosenbloom, N., & Watkins, K. R. (2013). Model support for forcing of the 8.2 ka event by meltwater from the Hudson Bay ice dome. *Climate Dynamics*, *41*(11), 2855–2873. https://doi.org/10.1007/s00382-013-1706-z

Wang, B., Kim, H.-J., Kikuchi, K., & Kitoh, A. (2011). Diagnostic metrics for evaluation of annual and diurnal cycles. *Climate Dynamics*, *37*(5–6), 941–955. https://doi.org/10.1007/s00382-010-0877-0

Wang, P. X., Wang, B., Cheng, H., Fasullo, J., Guo, Z. T., Kiefer, T., & Liu, Z. Y. (2014). The global monsoon across timescales: Coherent variability of regional monsoons. *Climate of the Past*, *10*(6), 2007–2052. https://doi.org/10.5194/cp-10-2007-2014

Wang, Y., Cheng, H., Edwards, R. L., He, Y., Kong, X., An, Z., et al. (2005). The Holocene Asian monsoon: Links to solar changes and North Atlantic climate. *Science*, *308*(5723), 854–857. https://doi.org/10.1126/science.1106296

Weijer, W., Cheng, W., Garuba, O. A., Hu, A., & Nadiga, B. T. (2020). CMIP6 models predict significant 21st century decline of the Atlantic meridional overturning circulation. *Geophysical Research Letters*, *47*(12), e2019GL086075. https://doi.org/10.1029/2019GL086075

Wiersma, A. P., & Renssen, H. (2006). Model–data comparison for the 8.2kaBP event: Confirmation of a forcing mechanism by catastrophic drainage of Laurentide Lakes. *Quaternary Science Reviews*, *25*(1–2), 63–88. https://doi.org/10.1016/j.quascirev.2005.07.009

Wiersma, A. P., Renssen, H., Goosse, H., & Fichefet, T. (2006). Evaluation of different freshwater forcing scenarios for the 8.2 ka BP event in a coupled climate model. *Climate Dynamics*, *27*(7–8), 831–849. https://doi.org/10.1007/s00382-006-0166-0

Williams, C. J. R., Guarino, M.-V., Capron, E., Malmierca-Vallet, I., Singarayer, J. S., Sime, L. C., et al. (2020). CMIP6/PMIP4 simulations of the mid-Holocene and Last Interglacial using HadGEM3: Comparison to the pre-industrial era, previous model versions and proxy data. *Climate of the Past*, *16*(4), 1429–1450. https://doi.org/10.5194/cp-16-1429-2020

Wood, C. T., Johnson, K. R., Lewis, L. E., Wright, K., Wang, J. K., Borsato, A., et al. (2023). High-resolution, multiproxy speleothem record of the 8.2 ka event from mainland southeast Asia. *Paleoceanography and Paleoclimatology*, *38*(12), e2023PA004675. https://doi.org/10.1029/2023PA004675

Wurtzel, J. B., Abram, N. J., Lewis, S. C., Bajo, P., Hellstrom, J. C., Troitzsch, U., & Heslop, D. (2018). Tropical Indo-Pacific hydroclimate response to North Atlantic forcing during the last deglaciation as recorded by a speleothem from Sumatra, Indonesia. *Earth and Planetary Science Letters*, *492*, 264–278. https://doi.org/10.1016/j.epsl.2018.04.001

Yeung, N. K.-H., Menviel, L., Meissner, K. J., Choudhury, D., Ziehn, T., & Chamberlain, M. A. (2024). Last Interglacial subsurface warming on the Antarctic shelf triggered by reduced deep-ocean convection. *Communications Earth and Environment*, *5*(1), 212. https://doi.org/10.1038/s43247-024-01383-x

Yeung, N. K.-H., Menviel, L., Meissner, K. J., Taschetto, A. S., Ziehn, T., & Chamberlain, M. (2021). Land–sea temperature contrasts at the Last Interglacial and their impact on the hydrological cycle. *Climate of the Past*, *17*(2), 869–885. https://doi.org/10.5194/cp-17-869-2021

Ziehn, T., Chamberlain, M. A., Law, R. M., Lenton, A., Bodman, R. W., Dix, M., et al. (2020). The Australian Earth system model: ACCESS-ESM1.5. *Journal of Southern Hemisphere Earth Systems Science*, *70*(1), 193–214. https://doi.org/10.1071/ES19035

Zwier, M., Van Der Bilt, W. G., De Stigter, H., & Bjune, A. E. (2022). Pollen evidence of variations in Holocene climate and southern hemisphere westerly wind strength on sub-Antarctic SouthSouth Georgia. *The Holocene*, *32*(3), 147–158. https://doi.org/10.1177/09596836211060495

Zwier, M., Van Der Bilt, W. G. M., Schneider, T., D'Andrea, W. J., Bakke, J., Van Der Putten, N., & Bjune, A. E. (2024). Holocene changes in the position of the Southern Hemisphere Westerlies recorded by long-distance transport of pollen to the Kerguelen Islands. *Quaternary Science Reviews*, *330*, 108595. https://doi.org/10.1016/j.quascirev.2024.108595

References From the Supporting Information

Arz, H. W., Gerhardt, S., Patzold, J., & Rohl, U. (2001). Millennial-scale changes of surface- and deep-water flow in the western tropical Atlantic linked to northern hemisphere high-latitude climate during the Holocene. *Geology*, *29*(3), 239–242. https://doi.org/10.1130/0091-7613(2001)029<0239:MSCOSA>2.0.CO;2

Baker, P. A., Fritz, S. C., Garland, J., & Ekdahl, E. (2005). Holocene hydrologic variation at Lake Titicaca, Bolivia/Peru, and its relationship to North Atlantic climate variation. *Journal of Quaternary Science*, *20*(7–8), 655–662. https://doi.org/10.1002/jqs.987

Bernal, J. P., Cruz, F. W., Stríkis, N. M., Wang, X., Deininger, M., Catunda, M. C. A., et al. (2016). High-resolution Holocene South American monsoon history recorded by a speleothem from Botuverá Cave, Brazil. *Earth and Planetary Science Letters*, *450*, 186–196. https://doi.org/10.1016/j.epsl.2016.06.008

Chazen, C. R., Altabet, M. A., & Herbert, T. D. (2009). Abrupt mid-Holocene onset of centennial-scale climate variability on the Peru-Chile Margin. *Geophysical Research Letters*, *36*(18), L18704. https://doi.org/10.1029/2009GL039749

Cheng, H., Fleitmann, D., Edwards, R. L., Wang, X., Cruz, F. W., Auler, A. S., et al. (2009). Timing and structure of the 8.2 kyr BP event inferred from δ18O records of stalagmites from China, Oman, and Brazil. *Geology*, *37*(11), 1007–1010. https://doi.org/10.1130/G30126A.1

Cremer, H., Heiri, O., Wagner, B., & Wagner-Cremer, F. (2007). Abrupt climate warming in East Antarctica during the early Holocene. *Quaternary Science Reviews*, *26*(15–16), 2012–2018. https://doi.org/10.1016/j.quascirev.2006.09.011

Conroy, J. L., Overpeck, J. T., Cole, J. E., Shanahan, T. M., & Steinitz-Kannan, M. (2008). Holocene changes in eastern tropical Pacific climate inferred from a Galapagos lake sediment record. *Quaternary Science Reviews*, *27*(11–12), 1166–1180. https://doi.org/10.1016/j.quascirev.2008.02.015

Denis, D., Crosta, X., Schmidt, S., Carson, D. S., Ganeshram, R. S., Renssen, H., et al. (2009). Holocene glacier and deep water dynamics, Adélie Land region, East Antarctica. *Quaternary Science Reviews*, *28*(13–14), 1291–1303. https://doi.org/10.1016/j.quascirev.2008.12.024

Duan, P., Li, H., Sinha, A., Voarintsoa, N. R. G., Kathayat, G., Hu, P., et al. (2021). The timing and structure of the 8.2 ka event revealed through high-resolution speleothem records from northwestern Madagascar. *Quaternary Science Reviews*, *268*, 107104. https://doi.org/10.1016/j.quascirev.2021.107104

Garcin, Y., Vincens, A., Williamson, D., Guiot, J., & Buchet, G. (2006). Wet phases in tropical southern Africa during the last glacial period. *Geophysical Research Letters*, *33*(7). https://doi.org/10.1029/2005GL025531

Haberzettl, T., Corbella, H., Fey, M., Janssen, S., Lücke, A., Mayr, C., et al. (2007). Lateglacial and Holocene wet-dry cycles in southern Patagonia: Chronology, sedimentology and geochemistry of a lacustrine record from Laguna Potrok Aike, Argentina. *The Holocene*, *17*(3), 297–310. https://doi.org/10.1177/0959683607076437

Hodell, D. A., Kanfoush, S. L., Shemesh, A., Crosta, X., Charles, C. D., & Guilderson, T. P. (2001). Abrupt cooling of Antarctic surface waters and sea ice expansion in the South Atlantic sector of the southern ocean at 5000 cal yr BP. *Quaternary Research*, *56*(2), 191–198. https://doi.org/10.1006/qres.2001.2252

Holmgren, K., Lee-Thorp, J. A., Cooper, G. R. J., Lundblad, K., Partridge, T. C., Scott, L., et al. (2003). Persistent millennial-scale climatic variability over the past 25,000 years in Southern Africa. *Quaternary Science Reviews*, *22*(21–22), 2311–2326. https://doi.org/10.1016/S0277-3791(03)00204-X

Johnson, T. C., Brown, E. T., McManus, J., Barry, S., Barker, P., & Gasse, F. (2002). A high-resolution paleoclimate record spanning the past 25,000 years in southern east Africa. *Science*, *296*(113–114), 131–132. https://doi.org/10.1126/science.1070057

Jouzel, J., Masson-Delmotte, V., Cattani, O., Dreyfus, G., Falourd, S., Hoffmann, G., et al. (2007). Orbital and millennial Antarctic climate variability over the past 800,000 years. *Science*, *317*(5839), 793–796. https://doi.org/10.1126/science.1141038

Kulbe, T., Melles, M., Verkulich, S. R., & Pushina, Z. V. (2001). East Antarctic climate and environmental variability over the last 9400 years inferred from marine sediments of the Bunger Oasis, Arctic. *Antarctic and Alpine Research*, *33*(2), 223–230. https://doi.org/10.1080/15230430.2001.12003425

Ljung, K., Björck, S., Renssen, H., & Hammarlund, D. (2008). South Atlantic island record reveals a South Atlantic response to the 8.2 kyr event. *Climate of the Past*, *4*(1), 35–45. https://doi.org/10.5194/cp-4-35-2008

Mayr, C., Wille, M., Haberzettl, T., Fey, M., Janssen, S., Lücke, A., et al. (2007). Holocene variability of the southern hemisphere westerlies in Argentinean Patagonia (52°S). *Quaternary Science Reviews*, *26*(5–6), 579–584. https://doi.org/10.1016/j.quascirev.2006.11.013

Moros, M., De Deckker, P., Jansen, E., Perner, K., & Telford, R. J. (2009). Holocene climate variability in the Southern Ocean recorded in a deep-sea sediment core off South Australia. *Quaternary Science Reviews*, *28*(19–20), 1932–1940. https://doi.org/10.1016/j.quascirev.2009.04.007

Moy, C. M. S. G. O., Rodbell, D. T., & Anderson, D. M. (2002). Variability of El Nino/southern oscillation activity at millennial timescales during the Holocene epoch. *Nature*, *420*(6912), 162–165. https://doi.org/10.1038/nature01194

Nielsen, S. H. H., Koç, N., & Crosta, X. (2004). Holocene climate in the Atlantic sector of the Southern Ocean: Controlled by insolation or oceanic circulation? *Geology*, *32*(4), 317–320. https://doi.org/10.1130/G20334.1

Petit, J. R., Jouzel, J., Raynaud, D., Barkov, N. I., Barnola, J.-M., Basile, I., et al. (1999). Climate and atmospheric history of the past 420,000 years from the Vostok ice core, Antarctica. *Nature*, *399*(6735), 429–436. https://doi.org/10.1038/20859

Rühlemann, C., Mulitza, S., Lohmann, G., Paul, A., Prange, M., & Wefer, G. (2004). Intermediate depth warming in the tropical Atlantic related to weakened thermohaline circulation: Combining paleoclimate data and modeling results for the last deglaciation. *Paleoceanography*, *19*(1). https://doi.org/10.1029/2003PA000948

Steig, E. J., Brook, E. J., White, J. W. C., Sucher, C. M., Bender, M. L., Lehman, S. J., et al. (1998). Synchronous climate changes in Antarctica and the North Atlantic. *Science*, *282*(5386), 92–95. https://doi.org/10.1126/science.282.5386.92

Stenni, B., Masson-Delmotte, V., Johnsen, S., Jouzel, J., Longinelli, A., Monnin, E., et al. (2001). An oceanic cold reversal during the last deglaciation. *Science*, *293*(5537), 2074–2077. https://doi.org/10.1126/science.1059702

Thompson, L. G., Mosley-Thompson, E., Davis, M. E., Henderson, K. A., Brecher, H. H., Zagorodnov, V. S., et al. (2002). Kilimanjaro ice core records: Evidence of Holocene climate change in tropical Africa. *Science*, *298*(5593), 589–593. https://doi.org/10.1126/science.1073198

van Breukelen, M. R., Vonhof, H. B., Hellstrom, J. C., Wester, W. C. G., & Kroon, D. (2008). Fossil dripwater in stalagmites reveals Holocene temperature and rainfall variation in Amazonia. *Earth and Planetary Science Letters*, *275*(1–2), 54–60. https://doi.org/10.1016/j.epsl.2008.07.060